A four-field resonant response model for tokamak plasmas with applications to pedestal physics

R. Fitzpatrick* and Y. Lin

Institute for Fusion Studies, Department of Physics,
University of Texas at Austin, Austin TX 78712, USA

1 Introduction

1.1 Resonant magnetic perturbations

Externally generated, static, *resonant magnetic perturbations* (RMPs) can drive magnetic reconnection in tokamak plasmas that are intrinsically stable to tearing perturbations [1, 2, 3, 4, 5]. RMPs arise naturally as a consequence of magnetic field-coil misalignments [6], but are sometimes deliberately applied to tokamak plasmas in order to suppress edge localized modes (ELMs) [7]. Driven reconnection is significant because it leads to the formation of magnetic island chains at so-called *rational* magnetic flux-surfaces within the plasma [8]. Such chains locally flatten the pressure profile, and, thereby, degrade the plasma energy confinement [9].

The analysis of the response of a tokamak plasma to an RMP is most efficiently formulated as an asymptotic matching problem in which the plasma is divided into two distinct regions [10]. In the so-called *outer region*, which comprises most of the plasma, the plasma perturbation is governed by the equations of linearized, marginally-stable, ideal-magnetohydrodynamics (MHD). However, these equations become singular on rational magnetic flux-surfaces at which the perturbed magnetic field resonates with the equilibrium field. In the *inner region*, which consists of a set of narrow layers centered on the various rational surfaces, non-ideal-MHD effects become important.

1.2 Four-field resonant response model

It is well known that single-fluid resistive-MHD offers a very poor description of the response of the inner region to the magnetic perturbation in the outer region. For instance, the strong diamagnetic flows present in tokamak plasmas imply that the electron and ion fluid velocities are significantly different from one another, necessitating a two-fluid treatment [11]. Moreover, resistive-MHD does not take into account the important ion sound-radius lengthscale below which electron and ion dynamics become decoupled from one another [12, 13]. Previously, Cole & Fitzpatrick [14] used the four-field model of Fitzpatrick & Waelbroeck [15], which consists of four coupled nonlinear partial differential equations, and which is based on the original four-field model of Hazeltine, Kotschenreuther & Morrison [16], to determine the linear two-fluid response of a resonant layer to the perturbation in the outer region. This treatment was extended in Ref. [17] to take into account the anomalously large perpendicular energy diffusivity present in tokamak plasmas.

In configuration space, the four-field models of Refs. [14] and [17] yield a set of resonant layer equations that can be expressed as *ten* coupled first-order linear ordinary differential equations (o.d.e.s) [18]. However, in Fourier space, the resonant layer equations can be written as *four* coupled first-order linear o.d.e.s [14]. It is clearly advantageous to solve the equations in Fourier space. In Refs. [14] and [17], an approximation is made by which one of the terms in the Fourier-transformed layer equations is neglected. This approximation, which

*rfitzp@utexas.edu

is valid in low-β plasmas, is such that the layer equation that governs the parallel ion dynamics decouples from the other three equations, effectively converting a four-field resonant response model into a three-field model. Furthermore, the three remaining layer equations can be combined to give a single second-order linear o.d.e. This second-order equation is most conveniently solved by means of a Riccati transformation that converts it into a first-order nonlinear o.d.e. [19, 20, 21]. The advantage of the Riccati approach is that it can deal with numerically problematic solutions that blow up as $\exp(p^2)$, or faster, at large p, where p is the Fourier-space variable.

Lee, Park & Na [18] recently demonstrated how to solve the full tenth-order four-field resonant layer equations in configuration space using a Riccati transformation. In the process, they discovered that, in a high-β plasma, the RMP rotation frequency (as seen in the local $\mathbf{E}\times\mathbf{B}$ frame at the rational surface) at which the electromagnetic torque exerted on the plasma in the immediate vicinity of the resonant layer passes through zero is shifted in the ion diamagnetic direction from the electron diamagnetic frequency. This result is significant because there is some experimental evidence for such a shift [22].

The first aim of this paper is to demonstrate how the calculation of Lee et alia can be reimplemented in Fourier space. The Fourier version of the calculation is more convenient, from a numerical point of view, because it involves the solution of a fourth-order, rather than a tenth-order, system of equations.

1.3 Magnetically diverted plasmas

The safety-factor profile of a magnetically diverted tokamak plasma diverges logarithmically as the magnetic separatrix (a.k.a. the last closed magnetic flux-surface) is approached. At first sight, this suggests that, when determining the response of such a plasma to an RMP, it is necessary to include an infinite number of rational magnetic flux-surfaces (at which the RMP resonates with the equilibrium magnetic field) in the calculation, the majority of which lie very close to the separatrix. In fact, as was demonstrated in Ref. [23], when finite plasma resistivity is taken into account, this turns out not to be the case. Instead, it is only necessary to include rational surfaces that lie in the region $0<\Psi<1-\epsilon_c$, where Ψ is the normalized poloidal magnetic flux, and $0<\epsilon_c\ll 1$. Moreover, the value of ϵ_c can be calculated from the plasma parameters at the edge of the discharge.

The analysis of Ref. [23] was based on the three-field resonant response model of Refs. [14] and [17]. The second aim of this paper is to generalize this analysis by employing the new Fourier-space four-field resonant response model.

2 Asymptotic matching

2.1 Plasma equilibrium

Consider a large aspect-ratio tokamak plasma equilibrium whose magnetic flux-surfaces map out (almost) concentric circles in the poloidal plane. Such an equilibrium can be approximated as a periodic cylinder [4]. Let r, θ, z be right-handed cylindrical coordinates. The magnetic axis corresponds to $r=0$, and the plasma boundary to $r=a$, where a is the simulated minor radius of the plasma. The system is assumed to be periodic in the z-direction with periodicity length $2\pi\,R_0$, where R_0 is the simulated major radius of the plasma. The safety-factor profile takes the form $q(r)=r\,B_z/[R_0\,B_\theta(r)]$, where B_z is the constant "toroidal" magnetic field-strength, and $B_\theta(r)$ is the poloidal magnetic field-strength. The equilibrium poloidal and toroidal magnetic fluxes (divided by 2π) are written $\psi_p(r)=B_z\int_0^r r'/q(r')\,dr'$ and $\psi_t(r)=B_z\,r^2/2$, respectively. The standard large aspect-ratio tokamak orderings, $r/R_0\ll 1$ and $B_\theta/B_z\ll 1$, are adopted.

2.2 Outer region

Consider a static (in the laboratory frame) magnetic perturbation that has m periods in the poloidal direction, and n periods in the toroidal direction. The response of the plasma to the perturbation is governed by the linearized equations of marginally-stable ideal-MHD everywhere in the plasma, apart from a (radially) narrow layer centered on the rational surface whose minor radius, r_s, is such that $q(r_s)=m/n$ [10].

Regime	Q_e	Q_i	c_β	D	P_E	P_φ
HRi	-1.0	1.0	1.0	10.0	1.0	$1.0\times10^{+0}$
HRii	-1.0	1.0	1.0	10.0	1.0	1.0×10^{-1}
RIii	-0.15	0.15	1.0	1.0	1.0	1.0×10^{-4}
VRii	-0.15	0.15	1.0	0.1	1.0	$1.0\times10^{+0}$

Table 1: The normalized layer parameters used in the benchmark comparisons shown in Figs. 1–4.

The perturbed magnetic field is written $\delta\mathbf{B}\simeq\nabla\delta\psi\times\mathbf{e}_z$, where $\delta\psi(r,\theta,\varphi)=\delta\psi(r)\,\exp[\,\mathrm{i}\,(m\,\theta-n\,\varphi)]$, and $\varphi=z/R_0$ is a simulated toroidal angle. In the outer region (i.e., everywhere in the plasma apart from the resonant layer), the perturbed helical magnetic flux, $\delta\psi(r)$, satisfies the *cylindrical tearing mode equation* [24, 25],

$$\frac{d^2\delta\psi}{dr^2}+\frac{1}{r}\,\frac{d\delta\psi}{dr}-\frac{m^2}{r^2}\,\delta\psi-\frac{J_z'\,\delta\psi}{r\,(1/q-n/m)}=0, \tag{1}$$

where $J_z(r)=R_0\,\mu_0\,j_z(r)/B_z$, and $j_z(r)$ is the equilibrium "toroidal" current density. Here, $'\equiv d/dr$.

In general, the solution of Eq. (1) that satisfies physical boundary conditions at the magnetic axis and the plasma boundary is such that $\delta\psi(r)$ is continuous across the rational surface, whereas $d\delta\psi/dr$ is discontinuous. The discontinuity of $d\delta\psi/dr$ across the rational surface is indicative of the presence of a helical current sheet at the surface. The complex quantity $\Psi_s=\delta\psi(r_s)$ determines the amplitude and phase of the reconnected helical magnetic flux at the rational surface, whereas the complex quantity

$$\Delta\Psi_s=\left[r\,\frac{d\delta\psi}{dr}\right]_{r_{s-}}^{r_{s+}} \tag{2}$$

parameterizes the amplitude and phase of the helical current sheet [4].

The solution of the cylindrical tearing mode equation in the outer region, in the presence of an externally generated RMP (with m periods in the poloidal direction and n periods in the toroidal direction), leads to the *tearing mode dispersion relation* [4, 10]

$$\Delta\Psi_s-E_{ss}\,\Psi_s=-E_{ss}\,\Psi_v, \tag{3}$$

where E_{ss} is a real dimensionless quantity known as the *tearing stability index* [10]. Moreover, Ψ_v is the so-called *vacuum flux*, and is defined as the reconnected magnetic flux that would be driven at the rational surface by the RMP were the plasma intrinsically tearing-stable (i.e., $E_{ss}<0$), and were there no current sheet at the rational surface (i.e., $\Delta\Psi_s=0$) [4].

In the following, it is assumed that $E_{ss}<0$, which implies that the tearing mode that reconnects magnetic flux at the rational surface is intrinsically stable. In this case, any magnetic reconnection that takes place at the surface is entirely due to the RMP.

2.3 Inner region

The current sheet at the rational surface is resolved by employing a extended-MHD resonant response model in the inner region (i.e., the region of the plasma in the immediate vicinity of the rational surface) to determine the complex *layer response index*, Δ_s. Asymptotic matching between the solutions in the inner and the outer regions yields

$$\Delta_s=\frac{\Delta\Psi_s}{\Psi_s}. \tag{4}$$

The previous two equations lead to the *plasma response equation*,

$$\Psi_s=\frac{\Psi_v}{1+\Delta_s/(-E_{ss})}. \tag{5}$$

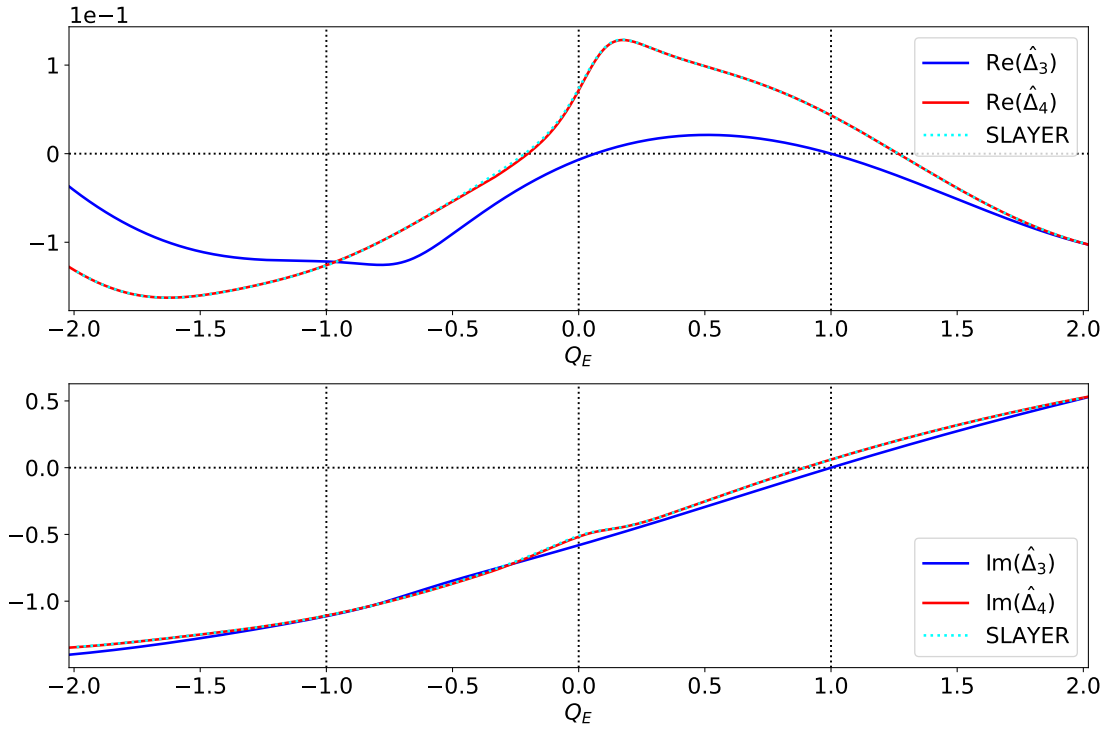

Figure 1: The scaled layer response index, $\hat{\Delta}$, plotted as a function of the normalized $\mathbf{E}\times\mathbf{B}$ frequency, Q_E, in the first Hall-resistive (HRi) response regime. (See Table 1.) $\hat{\Delta}_3$ is the response index predicted by the three-field Fourier-space response model of Ref. [17]. $\hat{\Delta}_4$ is the response index predicted by the four-field Fourier-space response model specified in Appendix A. SLAYER is the response index predicted by the four-field configuration-space response model of Ref. [18]. The three vertical lines indicate the ion fluid resonance, $Q_E+Q_i=0$, the MHD fluid resonance, $Q_E=0$, and the electron fluid resonance, $Q_E+Q_e=0$, respectively, in order from the left to the right.

Note that if $|\Delta_s|/(-E_{ss})\ll 1$ then $\Psi_s\simeq\Psi_v$ and $\Delta\Psi_s\simeq 0$, which is termed a *vacuum response*. On the other hand, if $|\Delta_s|/(-E_{ss})\gg 1$ then $|\Psi_s|\ll|\Psi_v|$, which is termed an *ideal response*. In the vacuum response regime, the current sheet that is excited in the resonant layer is too feeble to prevent driven magnetic reconnection, and the reconnected flux at the rational surface is the same as that which would be driven if there were no plasma present at the surface. On the other hand, in the ideal response regime, the current sheet excited in the layer is large enough to almost completely suppress driven magnetic reconnection, which implies that the response of the plasma is equivalent to that which would occur if the ideal-MHD flux freezing constraint, $\Psi_s=0$, were imposed at the rational surface [23].

3 Fourier-space four-field resonant response model

3.1 Introduction

The Fourier-space four-field resonant response model employed in this paper is described in detail in Appendix A.

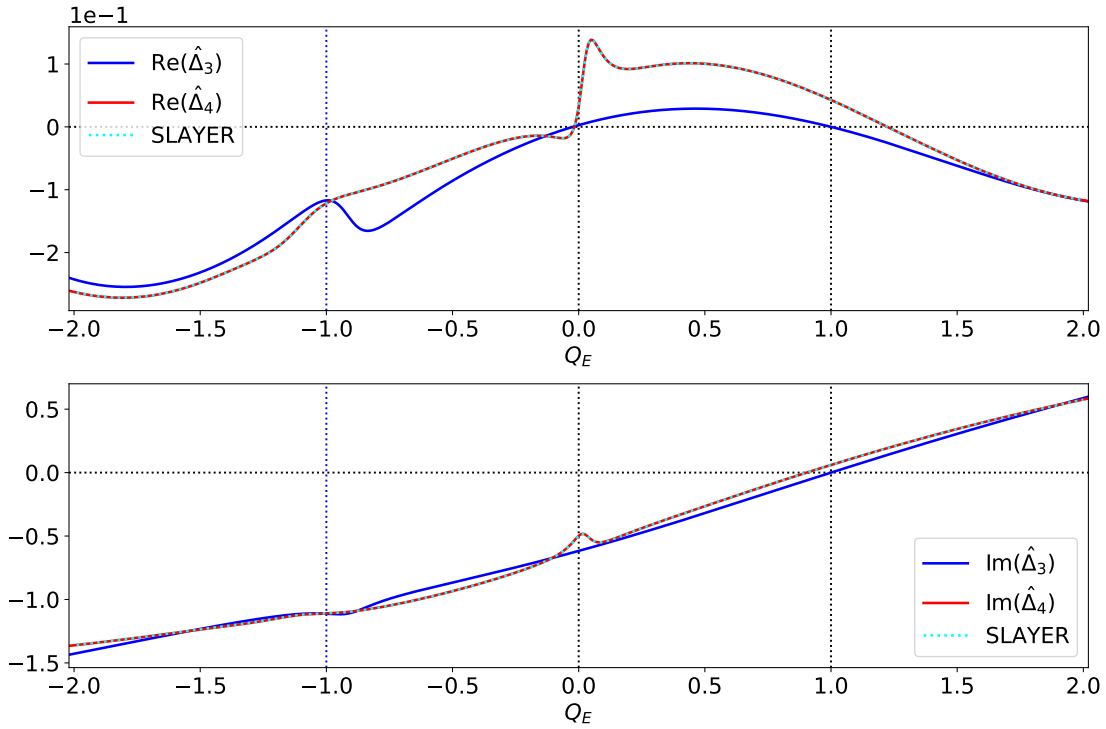

Figure 2: The scaled layer response index, $\hat{\Delta}$, plotted as a function of the normalized $\mathbf{E}\times\mathbf{B}$ frequency, Q_E, in the second Hall-resistive (HRii) response regime. See Table 1 and the caption to Fig. 1.

3.2 Dimensionless parameters

All four-field resonant response models are defined by the following seven dimensionless parameters: $Q_E = -S^{1/3}\,n\,\omega_E\,\tau_H$, $Q_e = -S^{1/3}\,n\,\omega_{*\,e}\,\tau_H$, $Q_i = -S^{1/3}\,n\,\omega_{*\,i}\,\tau_H$, $c_\beta = \sqrt{\beta/(1+\beta)}$, $D = S^{1/3}\,\iota_e^{1/2}\,\hat{d}_\beta$, $P_E = \tau_R/\tau_E$, and $P_\varphi = \tau_R/\tau_\varphi$. Here, τ_R is the resistive diffusion timescale, τ_H the hydrodynamic timescale, τ_E the energy confinement timescale, τ_φ the momentum confinement timescale, $S = \tau_R/\tau_H$ the Lundquist number, ω_E the $\mathbf{E}\times\mathbf{B}$ frequency, $\omega_{*\,e}$ the electron diamagnetic frequency, $\omega_{*\,i}$ the ion diamagnetic frequency, $\sqrt{\beta} = \sqrt{(5/3)\,\mu_0\,p/B_z}$ the ratio of the sound speed to the Alfvén speed, p the plasma pressure, $d_\beta = c_\beta\,d_i$ the ion sound-radius, and d_i the collisionless ion skin-depth. Moreover, P_E and P_φ are magnetic Prandtl numbers, $\iota_e = -\omega_{*\,e}/(\omega_{*\,i}-\omega_{*\,e})$, and $\hat{d}_\beta = d_\beta/r_s$. All quantities are evaluated at the rational surface. (See Appendix A for more detailed definitions.)

Note that the previous definitions are slightly different to those adopted in Ref. [18]. We can convert our dimensionless parameter into into those used by Lee et alia by letting $Q_E \to Q$, $Q_e \to -Q_{*\,e}$, $Q_i \to -Q_{*\,i}$, $\iota_e \to 1/(1+\tau)$, $P_E \to c_\beta^2$, and $P_\varphi \to P$.

3.3 Method of solution

After linearization and Fourier transformation (with respect to $x = r - r_s$), our four-field equations can be converted into the Ricatti matrix differential equation

$$p\,\frac{d\underline{\underline{W}}}{dp} = \underline{\underline{W}} - \underline{\underline{W}}\,\underline{\underline{W}} - \underline{\underline{E}}\,\underline{\underline{W}} + \underline{\underline{F}}. \tag{6}$$

Here, p is the Fourier transform variable, and $\underline{\underline{W}}(p)$ the 2×2 solution matrix. The elements of the 2×2 matrices $\underline{\underline{E}}(p)$ and $\underline{\underline{F}}(p)$ are specified in Eqs. (89)–(92) and (93)–(96), respectively. The method of solution

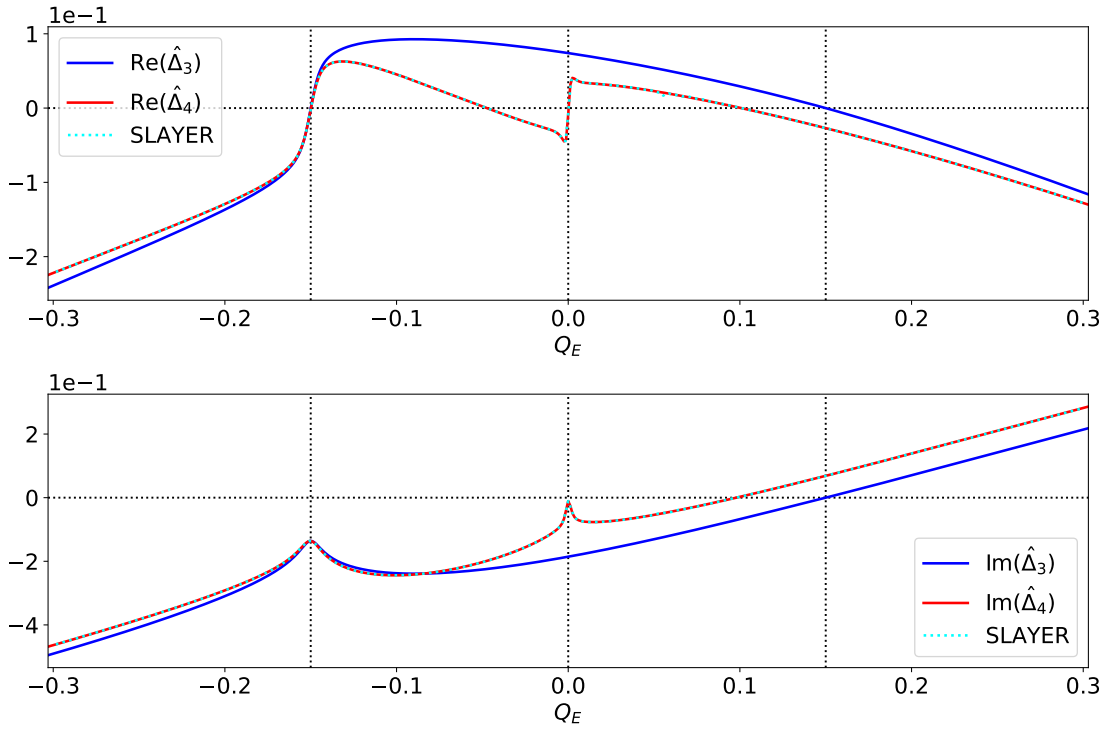

Figure 3: The scaled layer response index, $\hat{\Delta}$, plotted as a function of the normalized $\mathbf{E}\times\mathbf{B}$ frequency, Q_E, in the second resistive-inertial (RIii) response regime. See Table 1 and the caption to Fig. 1.

is as follows. A solution of the Ricatti equation is launched from a large (with respect to unity) value of p, with the initial solution matrix specified in Eq. (153), and is then integrated to a small (with respect to unity) value of p. The *scaled layer response index*, $\hat{\Delta}$, is then deduced from the small-p elements of the solution matrix by means of Eq. (117). The true layer response index is $\Delta_s = S^{1/3}\,\hat{\Delta}$.

3.4 Benchmarking against SLAYER

Our first task is to benchmark the results of our Fourier-space calculation of $\hat{\Delta}$ against the results of the configuration-space calculation performed by Lee et alia. The latter calculation has been implemented in the SLAYER code [18, 20].

Figures 1–4 show the scaled layer response index, $\hat{\Delta}$, calculated as a function of the normalized $\mathbf{E}\times\mathbf{B}$ frequency, Q_E, by three different solution methods, in four of the analytic layer response regimes identified in Ref. [14]. The dimensionless layer parameters used in the four calculations are specified in Table 1. The first solution method involves using the Fourier-space analysis of Ref. [17]. In this analysis, the term involving c_β^2 is neglected in Eq. (44). Consequently, Eq. (46) decouples from Eqs. (43)–(45), which effectively converts a four-field response model (the four fields being $\bar{\psi}$, $\bar{N}$, $\bar{\phi}$, and $\bar{V}$) into a three-field response model (the three fields being $\bar{\psi}$, $\bar{N}$, and $\bar{\phi}$). The second solution method involves using the Fourier-space analysis set out in Appendix A. This method solves Eqs. (43)–(46), with no neglected terms, and thus constitutes a four-field response model. The first two methods have been implemented in the TJ code [26, 27]. The third solution method involves using the configuration-space analysis of Ref. [18], which is implemented in the SLAYER code [20]. Solution methods two and three constitute equivalent four-field response models.

It is clear from Figs. 1–4 that the second and third solution methods yield exactly the same results. This is remarkable because the second method involves solving four coupled first-order o.d.e.s in Fourier space,

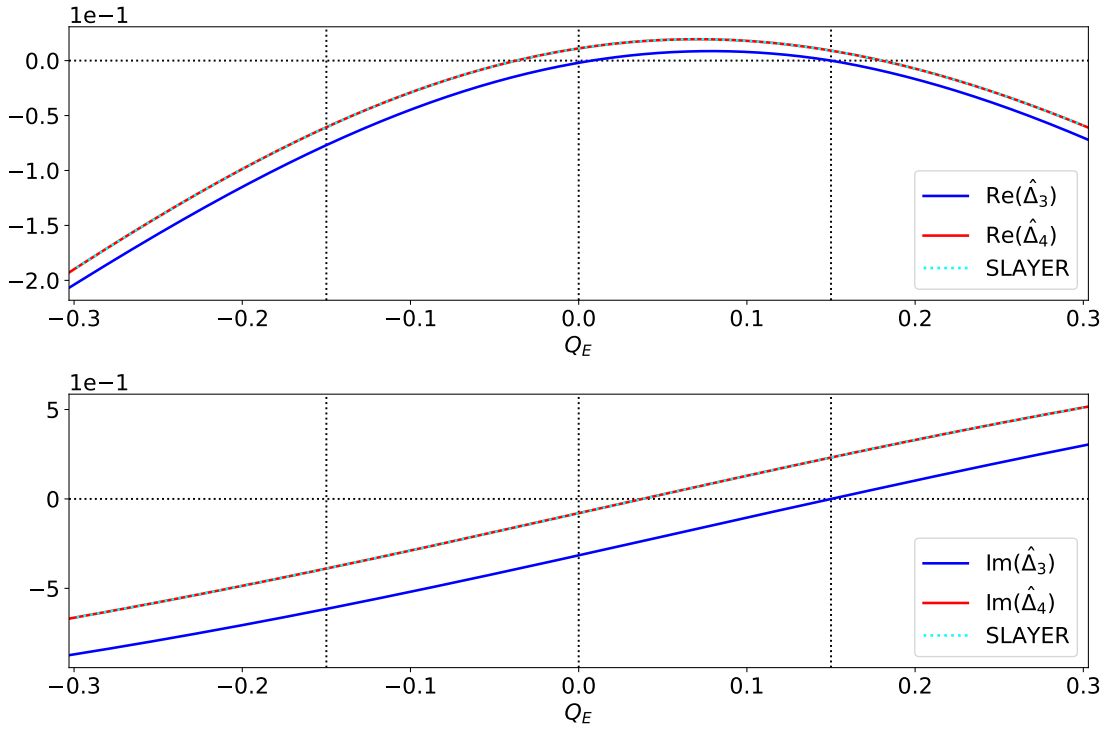

Figure 4: The scaled layer response index, $\hat{\Delta}$, plotted as a function of the normalized $\mathbf{E}\times\mathbf{B}$ frequency, Q_E, in the second viscous-resistive (VRii) response regime. See Table 1 and the caption to Fig. 1.

whereas the third involves solving ten coupled first-order o.d.e.s in configuration space. Moreover, as is clear from a comparison of Appendix A and Ref. [18], the analysis that leads to the four coupled equations in the former method is radically different from, and completely independent of, that which leads to the ten coupled equations in the the latter method. It follows that the two solution methods constitute strong independent checks on one another. Hence, we can be confident that the two methods are valid, and also that they have been implemented correctly in the TJ and SLAYER codes.

3.5 Effect of c_β

Figures 1–4 allow us to assess the consequences of neglecting the term involving c_β^2 in Eq. (44) by looking at the difference between $\hat{\Delta}_4$ and $\hat{\Delta}_3$. Obviously, this neglect is not going to make a difference if the ion sound parameter, c_β, is much less than unity, which explains why the rather large value, $c_\beta = 1$, is used in the calculations shown in the figures. (See Table 1.) It can be seen from the figures that the neglect of the c_β^2 term has a larger relative effect on the real part of the scaled layer response index than on the imaginary part. Furthermore, Figs. 2 and 3 indicate that if the c_β^2 term is neglected then the plasma response model fails to capture resonant behavior that occurs, in some response regimes, close to the MHD-fluid resonance ($Q_E = 0$). All four figures indicate that if the c_β^2 term is neglected then the imaginary part of the response index passes through zero exactly at the electron fluid resonance ($Q_E + Q_e = 0$). This implies that the electromagnetic torque exerted by the RMP on the plasma in the resonant layer is zero at the electron fluid resonance. However, as is clear from the figures, when the c_β^2 term is retained then the Q_E value at which $\mathrm{Im}(\hat{\Delta}) = 0$ is shifted from the electron fluid resonance in the ion diamagnetic direction [i.e., $\mathrm{Im}(\hat{\Delta}) = 0$ when $Q_E + Q_e < 0$] [18].

Figure 5 shows the difference between the scaled layer response index predicted by the three-field Fourier-

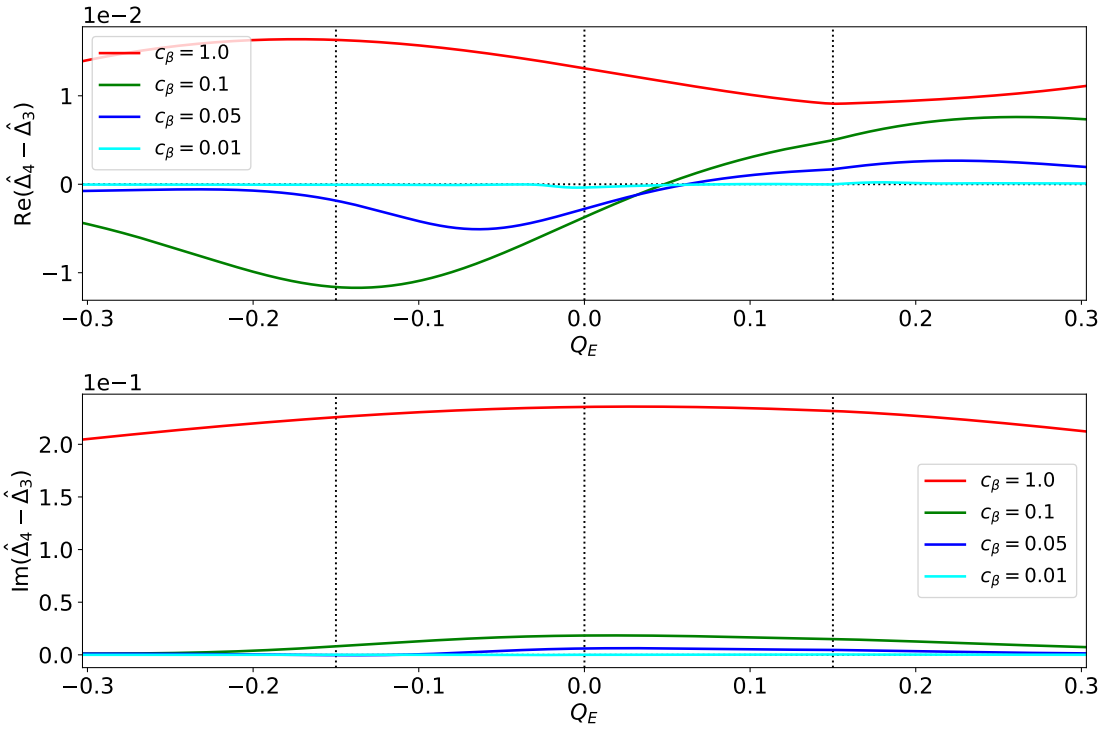

Figure 5: The difference between the scaled layer response indices predicted by the three-field and the four-field Fourier-space resonant response models plotted as a function of the normalized $\mathbf{E} \times \mathbf{B}$ frequency, Q_E. The calculations are performed in the VRii regime of Table 1, but for various different values of c_β. See the caption to Fig. 1.

space resonant response model of Ref. [17] and the four-field Fourier-space resonant response model of Appendix A. The calculations are performed using the Q_e, Q_i, D, P_E, and P_φ values associated with the VRii regime of Table 1, and for various different values of c_β. It can, again, be seen that finite c_β has a larger relative effect on the real part of the response index than on the imaginary part. It can also be seen that the difference between the predictions of the two models is an increasing function of increasing c_β, and that the difference is essentially negligible for c_β values less than 0.01.

Figure 6 shows the critical value of the normalized electron fluid rotation frequency at the rational surface, $Q_E + Q_e$, at which the imaginary part of the layer response index, $\mathrm{Im}(\hat{\Delta})$, is zero, plotted as a function of c_β. The calculations are performed using the Q_e, Q_i, D, P_E, and P_φ values associated with the HRi, HRii, RIii, and VRii regimes of Table 1. As is well known [4, 5], the nonlinear electromagnetic torque exerted by the RMP on the plasma in the immediate vicinity of the rational surface modifies the $\mathbf{E} \times \mathbf{B}$ frequency at the rational surface in such a manner as to reduce $\mathrm{Im}(\hat{\Delta})$ to a very small value. In fact, there is a critical RMP amplitude above which the normalized $\mathbf{E} \times \mathbf{B}$ frequency at the surface, Q_E, "locks" to the value that makes $\mathrm{Im}(\hat{\Delta})$ (almost) zero [5]. As is clear from the figure, when $c_\beta = 0$ the surface locks to the value of Q_E that makes $Q_E + Q_e = 0$. In other words, the nonlinear electromagnetic torque acts to bring the electron fluid at the rational surface to rest in the laboratory frame. However, the figure also indicates that at finite c_β the surface locks to a negative value of $Q_E + Q_e$, which implies that the electromagnetic torque acts to bring the plasmas into a state in which the electron and ion fluids at the rational surface rotate in opposite directions. As c_β increases the residual rotation frequency of the electron fluid [i.e., $(Q_E + Q_e)_{\rm crit}$] increases.

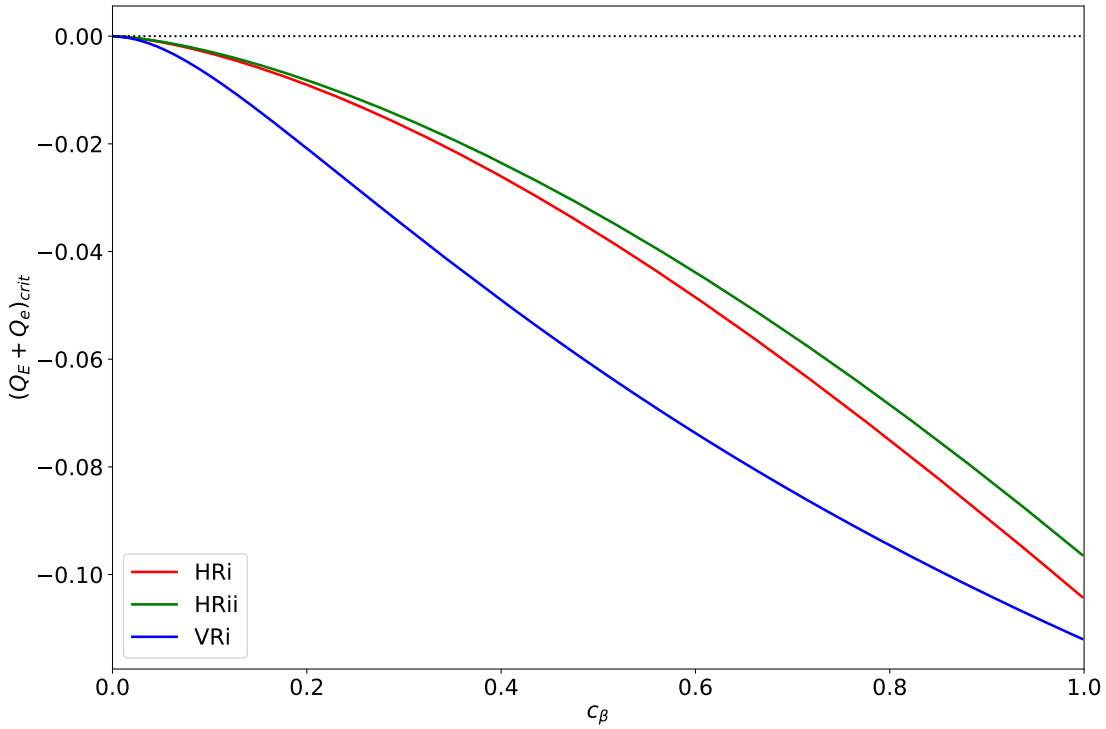

Figure 6: The critical value of the normalized electron fluid rotation frequency at the rational surface, $Q_E + Q_e$, at which the imaginary part of the layer response index is zero, plotted as a function of c_β, for the four response regimes specified in Table 1.

Acknowledgements

The authors would like to thank Y. Lee, J.-K. Park, J. Waybright, and D. Burgess for help benchmarking the results of this paper against those of Ref. [18].

Funding

This research was supported by the U.S. Department of Energy, Office of Science, Office of Fusion Energy Sciences, under contract DE-FG02-04ER54742.

Data availability statement

The data that support the findings of this study are available from the corresponding author upon reasonable request.

A Fourier-space four-field resonant plasma response model

A.1 Fundamental definitions

The plasma is assumed to consist of two species. First, electrons of mass m_e, electrical charge $-e$, number density n_e, and temperature T_e. Second, ions of mass m_i, electrical charge $+e$, number density n_e, and

temperature T_i. Let $p = n_e\,(T_e + T_i)$ be the total plasma pressure.

Let r_s be the minor radius of the rational surface. It is helpful to define $n_0 = n_e(r_s)$, $p_0 = p(r_s)$,

$$\eta_e = \left.\frac{d\ln T_e}{d\ln n_e}\right|_{r=r_s}, \tag{7}$$

$$\eta_i = \left.\frac{d\ln T_i}{d\ln n_e}\right|_{r=r_s}, \tag{8}$$

$$\iota = \left(\frac{T_e}{T_i}\right)_{r=r_s}\left(\frac{1+\eta_e}{1+\eta_i}\right) = \left(\frac{dp_e}{dp_i}\right)_{r_s}, \tag{9}$$

where $n_e(r)$, $p(r)$, $p_e(r)$, $p_i(r)$, $T_e(r)$, and $T_i(r)$ refer to electron number density, total pressure, electron pressure, ion pressure, electron temperature, and ion temperature profiles, respectively, in the absence of the magnetic perturbation.

For the sake of simplicity, the perturbed electron and ion temperature profiles are assumed to be functions of the perturbed electron number density profile in the immediate vicinity of the rational surface. In other words, $T_e = T_e(n_e)$ and $T_i = T_i(n_e)$. This implies that $p = p(n_e)$. The "MHD velocity", which is the velocity of a fictional MHD fluid [28], is defined $\mathbf{V} = \mathbf{V}_E + V_{\parallel\,i}\,\mathbf{b}$, where $\mathbf{V}_E$ is the $\mathbf{E}\times\mathbf{B}$ drift velocity, $V_{\parallel\,i}$ is the parallel component of the ion fluid velocity, $\mathbf{b} = \mathbf{B}/|\mathbf{B}|$, and $\mathbf{B}$ is the magnetic field-strength.

A.2 Fundamental fields

The four fundamental fields in our four-field model—namely, ψ, N, ϕ, and V—have the following definitions:

$$\nabla\psi = \frac{\mathbf{e}_\parallel\times\mathbf{B}}{r_s\,B_z}, \tag{10}$$

$$N = -\hat{d}_i\left(\frac{p-p_0}{B_z^2/\mu_0}\right), \tag{11}$$

$$\nabla\phi = \frac{\mathbf{e}_\parallel\times\mathbf{V}}{r_s\,V_A}, \tag{12}$$

$$V = \hat{d}_i\left(\frac{\mathbf{e}_\parallel\cdot\mathbf{V}}{V_A}\right). \tag{13}$$

Here, $\mathbf{e}_\parallel = (0,\,\epsilon/q_s,\,1)$, $\epsilon = r/R_0$, $q_s = m/n$, $V_A = (B_z/\sqrt{\mu_0\,n_0\,m_i})_{r_s}$, $d_i = \sqrt{m_i/(n_0\,e^{\,2}\,\mu_0)}_{r_s}$, and $\hat{d}_i = d_i/r_s$. Our model also employs the auxiliary field

$$J = -\frac{2\,\epsilon_s}{q_s} + \hat{\nabla}^2\psi, \tag{14}$$

where $\epsilon_s = r_s/R_0$, and $\hat{\nabla} = r_s\,\nabla$. Note that V_A is the *Alfvén speed* at the rational surface, whereas d_i is the *collisionless ion skin-depth*.

A.3 Fundamental equations

For the case of a static (in the laboratory frame) magnetic perturbation, the four-field model takes the form [15, 14, 17]:

$$0 = [\phi,\psi] - \iota_e\,[N,\psi] + \hat{\eta}_\parallel\,J + \hat{E}_\parallel, \tag{15}$$

$$0 = [\phi,N] + \hat{d}_\beta^{\,2}\,[J,\psi] + c_\beta^2\,[V,\psi] + \hat{\chi}_E\,\hat{\nabla}^2 N, \tag{16}$$

$$0 = [\phi,\hat{\nabla}^2\phi] - \frac{\iota_i}{2}\left(\hat{\nabla}^2[\phi,N] + [\hat{\nabla}^2\phi,N] + [\hat{\nabla}^2 N,\phi]\right) + [J,\psi] + \hat{\chi}_\varphi\,\hat{\nabla}^4(\phi + \iota_i\,N), \tag{17}$$

$$0 = [\phi,V] + [N,\psi] + \hat{\chi}_\varphi\,\hat{\nabla}^2 V. \tag{18}$$

Here, $[A,B] \equiv \hat{\nabla} A \times \hat{\nabla} B \cdot \mathbf{e}_\parallel$, $\iota_e = \iota/(1+\iota)$, $\iota_i = 1/(1+\iota)$, $\hat{t} = t/(r_s/V_A)$, $\hat{\eta}_\parallel = \eta_\parallel/(\mu_0\, r_s\, V_A)$, $\hat{E}_\parallel = E_\parallel/(B_z\, V_A)$, $\hat{\chi}_E = \chi_E/(r_s\, V_A)$, $\hat{\chi}_\varphi = \chi_\varphi/(r_s\, V_A)$, where $\eta_\parallel$ is the parallel plasma electrical resistivity at the rational surface, $E_\parallel$ the parallel inductive electric field that maintains the equilibrium toroidal plasma current in the vicinity of the rational surface, χ_E the anomalous perpendicular heat diffusivity at the rational surface, and χ_φ the anomalous perpendicular ion momentum diffusivity at the rational surface. Moreover, $d_\beta = c_\beta\, d_i$, and $\hat{d}_\beta = d_\beta/r_s$, where $c_\beta = [\beta/(1+\beta)]_{r_s}^{1/2}$, and $\beta = (5/3)\,\mu_0\, p_0/B_z^2$. Here, d_β is usually referred to as the *ion sound-radius*.

A.4 Matching to plasma equilibrium

The unperturbed plasma equilibrium is such that $\mathbf{B} = (0,\, B_\theta(r),\, B_z)$, $p = p(r)$, $\mathbf{V} = (0,\, V_E(r),\, V_z(r))$, where $V_E(r) \simeq -E_r/B_z$ is the (dominant θ-component of the) $\mathbf{E}\times\mathbf{B}$ velocity. Now, the resonant layer is assumed to have a radial thickness that is much smaller than r_s. Hence, we only need to evaluate plasma equilibrium quantities in the immediate vicinity of the rational surface. Equations (10)–(13) suggest that

$$\psi(\hat{x}) = \frac{\hat{x}^{\,2}}{2\,\hat{L}_s}, \tag{19}$$

$$N(\hat{x}) = -\hat{V}_*\,\hat{x}, \tag{20}$$

$$\phi(\hat{x}) = -\hat{V}_E\,\hat{x}, \tag{21}$$

$$V(\hat{x}) = \hat{V}_\parallel, \tag{22}$$

where $\hat{x} = (r-r_s)/r_s$, $\hat{L}_s = L_s/r_s$, $L_s = R_0\, q_s/s_s$, $\hat{V}_E = V_E(r_s)/V_A$, $\hat{V}_* = V_*(r_s)/V_A$, $V_*(r) = (dp/dr)/(e\, n_0\, B_z)$ is the (dominant θ-component of the) diamagnetic velocity, and $\hat{V}_\parallel = \hat{d}_i\, V_z(r_s)/V_A$. Here, $s_s = s(r_s)$ and $s(r) = d\ln q/d\ln r$. We also have

$$J(\hat{x}) = -\left(\frac{2}{s_s} - 1\right)\frac{1}{\hat{L}_s}, \tag{23}$$

and $\hat{E}_\parallel(\hat{x}) = (2/s_s - 1)\,(\hat{\eta}_\parallel/\hat{L}_s)$.

A.5 Derivation of linear layer equations

In accordance with Eqs. (19)–(23), let us write

$$\psi(\hat{x},\zeta) = \frac{\hat{x}^{\,2}}{2\,\hat{L}_s} + \tilde{\psi}(\hat{x})\,\mathrm{e}^{\,\mathrm{i}\,\zeta}, \tag{24}$$

$$\phi(\hat{x},\zeta) = -\hat{V}_E\,\hat{x} + \tilde{\phi}(\hat{x})\,\mathrm{e}^{\,\mathrm{i}\,\zeta}, \tag{25}$$

$$N(\hat{x},\zeta) = -\hat{V}_*\,\hat{x} + \iota_e\,\tilde{N}(\hat{x})\,\mathrm{e}^{\,\mathrm{i}\,\zeta}, \tag{26}$$

$$V(\hat{x},\zeta) = \hat{V}_\parallel + \iota_e\,\tilde{V}(\hat{x})\,\mathrm{e}^{\,\mathrm{i}\,\zeta}, \tag{27}$$

$$J(\hat{x},\zeta) = -\left(\frac{2}{s_s} - 1\right)\frac{1}{\hat{L}_s} + \hat{\nabla}^2\tilde{\psi}(\hat{x})\,\mathrm{e}^{\,\mathrm{i}\,\zeta}, \tag{28}$$

where $\zeta = m\,\theta - n\,\varphi$. Substituting Eqs. (24)–(28) into Eqs. (14)–(18), and only retaining terms that are first order in perturbed quantities, we obtain the following set of linear equations:

$$-\mathrm{i}\,n\,(\omega_E+\omega_{*\,e})\,\tau_H\,\tilde{\psi} = -\mathrm{i}\,\hat{x}\,(\tilde{\phi}-\tilde{N}) + S^{-1}\,\hat{\nabla}^2\tilde{\psi}, \tag{29}$$

$$-\mathrm{i}\,n\,\omega_E\,\tau_H\,\tilde{N} = \mathrm{i}\,n\,\omega_{*\,e}\,\tau_H\,\tilde{\phi} - \mathrm{i}\,\iota_e\,\hat{d}_\beta^2\,\hat{x}\,\hat{\nabla}^2\tilde{\psi} - \mathrm{i}\,c_\beta^2\,\hat{x}\,\tilde{V} + S^{-1}\,P_E\,\hat{\nabla}^2\tilde{N}, \tag{30}$$

$$-\mathrm{i}\,n\,(\omega_E+\omega_{*\,i})\,\tau_H\,\hat{\nabla}^2\tilde{\phi} = -\mathrm{i}\,\hat{x}\,\hat{\nabla}^2\tilde{\psi} + S^{-1}\,P_\varphi\,\hat{\nabla}^4\left(\tilde{\phi}+\frac{\tilde{N}}{\iota}\right), \tag{31}$$

$$-\mathrm{i}\,n\,\omega_E\,\tau_H\,\tilde{V} = -\mathrm{i}\,n\,\omega_{*\,e}\,\tau_H\,\tilde{\psi} - \mathrm{i}\,\hat{x}\,\tilde{N} + S^{-1}\,P_\varphi\,\hat{\nabla}^2\tilde{V}. \tag{32}$$

Here, $\tau_H = L_s/(m\,V_A)$ is the hydromagnetic time, $\omega_E = -(q_s/r_s)\,V_E(r_s) = -(d\Phi/d\psi_p)_{r_s}$ the $\mathbf{E}\times\mathbf{B}$ frequency, $\omega_{*\,e} = \iota_e\,(q_s/r_s)V_*(r_s) = [(dp_e/d\psi_p)/(e\,n_e)]_{r_s}$ the electron diamagnetic frequency, $\omega_{*\,i} = -\iota_i\,(m/r_s)V_*(r_s) = -[(dp_i/d\psi_p)/(e\,n_e)]_{r_s}$ the ion diamagnetic frequency, $\Phi(r)$ the equilibrium electrostatic potential, $S = \tau_R/\tau_H$ the Lundquist number, $\tau_R = \mu_0\,r_s^2/\eta_\parallel$ the resistive diffusion time, $\tau_E = r_s^2/\chi_E$ the energy confinement time, and $\tau_\varphi = r_s^2/\chi_\varphi$ the toroidal momentum confinement time. Furthermore, $P_E = \tau_R/\tau_E$ and $P_\varphi = \tau_R/\tau_\varphi$ are magnetic Prandtl numbers.

Let us define the stretched radial variable $X = S^{1/3}\,\hat{x}$. Assuming that $X \sim \mathcal{O}(1)$ in the layer (i.e., assuming that the layer thickness is roughly of order $S^{-1/3}\,r_s$), and making use of the fact that $S \gg 1$ in conventional tokamak plasmas, Eqs. (29)–(32) reduce to the following set of linear layer equations [14, 17]:

$$\mathrm{i}\,(Q_E+Q_e)\,\tilde{\psi} = -\mathrm{i}\,X\left(\tilde{\phi}-\tilde{N}\right) + \frac{d^2\tilde{\psi}}{dX^2}, \tag{33}$$

$$\mathrm{i}\,Q_E\,\tilde{N} = -\mathrm{i}\,Q_e\,\tilde{\phi} - \mathrm{i}\,D^2\,X\,\frac{d^2\tilde{\psi}}{dX^2} - \mathrm{i}\,c_\beta^2\,X\,\tilde{V} + P_E\,\frac{d^2\tilde{N}}{dX^2}, \tag{34}$$

$$\mathrm{i}\,(Q_E+Q_i)\,\frac{d^2\tilde{\phi}}{dX^2} = -\mathrm{i}\,X\,\frac{d^2\tilde{\psi}}{dX^2} + P_\varphi\,\frac{d^4}{dX^4}\left(\tilde{\phi}+\frac{\tilde{N}}{\iota}\right), \tag{35}$$

$$\mathrm{i}\,Q_E\,\tilde{V} = \mathrm{i}\,Q_e\,\tilde{\psi} - \mathrm{i}\,X\,\tilde{N} + P_\varphi\,\frac{d^2\tilde{V}}{dX^2}. \tag{36}$$

Here, $Q_E = -S^{1/3}\,n\,\omega_E\,\tau_H$, $Q_{e,i} = -S^{1/3}\,n\,\omega_{*\,e,i}\,\tau_H$, and $D = S^{1/3}\,\iota_e^{1/2}\,\hat{d}_\beta$.

If we write $P_E = c_\beta^2$ then Eqs. (33)–(36) become equivalent to the set of layer equations solved by Lee et alia. (To be slightly more exact, we get from our equations to those of Lee et alia by making the following transformation: $Q_E \to Q$, $Q_e \to -Q_{*\,e}$, $Q_i \to -Q_{*\,i}$, $\iota \to 1/\tau$, $P_E \to c_\beta^2$, $P_\varphi \to P$, $\tilde{\psi} \to -\tilde{\psi}$, $\tilde{N} \to \tilde{Z}$, $\tilde{\phi} \to \tilde{\phi}$, and $\tilde{V} \to -\tilde{V}_z$.)

The low-β approximation used in Refs. [14] and [17] involves neglecting the term containing c_β^2 in Eq. (34). This approximation decouples Eq. (36) from the three preceding equations, and effectively converts a four-field resonant response model into a three-field model. In the following, we shall not make use of this approximation.

A.6 Asymptotic matching

The linear layer equations, (33)–(36), possess tearing parity solutions characterized by the symmetry $\tilde{\psi}(-X) = \tilde{\psi}(X)$, $\tilde{N}(-X) = -\tilde{N}(X)$, $\tilde{\phi}(-X) = -\tilde{\phi}(X)$, $\tilde{V}(-X) = \tilde{V}(X)$. As is easily demonstrated, the asymptotic

behavior of the tearing parity solutions to Eqs. (33)–(36) are such that

$$\tilde{\psi}(X) \rightarrow \psi_0 \left[\frac{\hat{\Delta}}{2} \, |X| + 1 + \mathcal{O}\left(\frac{1}{X^2}\right) \right], \tag{37}$$

$$\tilde{\phi}(X) \rightarrow -\psi_0 \, Q_E \left[\frac{\hat{\Delta}}{2} \, \mathrm{sgn}(X) + \frac{1}{X} + \mathcal{O}\left(\frac{1}{X^2}\right) \right], \tag{38}$$

$$\tilde{N}(X) \rightarrow \psi_0 \, Q_e \left[\frac{\hat{\Delta}}{2} \, \mathrm{sgn}(X) + \frac{1}{X} + \mathcal{O}\left(\frac{1}{X^2}\right) \right], \tag{39}$$

$$\tilde{V}(X) \rightarrow \mathcal{O}\left(\frac{1}{X^3}\right) \tag{40}$$

as $|X| \rightarrow \infty$, where ψ_0 is an arbitrary constant. It follows from Eq. (4) that layer response index is

$$\Delta_s = S^{1/3} \, \hat{\Delta}. \tag{41}$$

A.7 Fourier transformation

Equations (33)–(36) are most conveniently solved in Fourier transform space [14]. Let

$$\bar{\phi}(p) = \int_{-\infty}^{\infty} \tilde{\phi}(X) \, \mathrm{e}^{-\mathrm{i}\, p\, X} \, dX, \tag{42}$$

et cetera. The Fourier transformed linear layer equations become

$$\mathrm{i}\,(Q_E + Q_e)\,\bar{\psi} = \frac{d}{dp}\left(\bar{\phi} - \bar{N}\right) - p^2\,\bar{\psi}, \tag{43}$$

$$\mathrm{i}\,Q_E\,\bar{N} = -\mathrm{i}\,Q_e\,\bar{\phi} - D^{\,2}\,\frac{d(p^2\,\bar{\psi})}{dp} + c_\beta^2\,\frac{d\bar{V}}{dp} - P_E\,p^2\bar{N}, \tag{44}$$

$$\mathrm{i}\,(Q_E + Q_i)\,p^2\,\bar{\phi} = \frac{d(p^2\,\bar{\psi})}{dp} - P_\varphi\,p^4\left(\bar{\phi} + \frac{\bar{N}}{\iota}\right), \tag{45}$$

$$\mathrm{i}\,Q_E\,\bar{V} = \mathrm{i}\,Q_e\,\bar{\psi} + \frac{d\bar{N}}{dp} - P_\varphi\,p^2\,\bar{V}, \tag{46}$$

where, for a tearing parity solution,

$$\bar{\phi}(p) - \bar{N}(p) \equiv \bar{Y}(p) \rightarrow \bar{Y}_0 \left[\frac{\hat{\Delta}}{\pi\,p} + 1 + \mathcal{O}(p) \right] \tag{47}$$

as $p \rightarrow 0$. Here, $\bar{Y}_0$ is an arbitrary constant.

Finally, if we define

$$\bar{J}(p) = p^2\,\bar{\psi}, \tag{48}$$

then Eqs. (43)–(46) can be converted into the following equivalent set of four coupled first-order o.d.e.s:

$$\frac{d\bar{Y}}{dp} = \left[\frac{\mathrm{i}\,(Q_E+Q_e)+p^2}{p^2}\right]\bar{J}, \tag{49}$$

$$\frac{d\bar{N}}{dp} = -\left(\frac{\mathrm{i}\,Q_e}{p^2}\right)\bar{J} + (\,\mathrm{i}\,Q_E + P_\varphi\,p^2)\,\bar{V}, \tag{50}$$

$$\frac{d\bar{J}}{dp} = [\,\mathrm{i}\,(Q_E+Q_i)\,p^2 + P_\varphi\,p^4]\,\bar{Y} + [\,\mathrm{i}\,(Q_E+Q_i)\,p^2 + \iota_e^{-1}\,P_\varphi\,p^4]\,\bar{N}, \tag{51}$$

$$\begin{aligned} c_\beta^2\,\frac{d\bar{V}}{dp} &= [\,\mathrm{i}\,Q_e + \mathrm{i}\,(Q_E+Q_i)\,D^2\,p^2 + D^2\,P_\varphi\,p^4]\,\bar{Y} \\ &\quad + \{\,\mathrm{i}\,(Q_E+Q_e) + [P_E + \mathrm{i}\,(Q_E+Q_i)\,D^2]\,p^2 + \iota_e^{-1}\,D^2\,P_\varphi\,p^4\}\,\bar{N}, \end{aligned} \tag{52}$$

Note that $\iota_e = -Q_e/(Q_i-Q_e)$.

A.8 Small argument expansion

Let us search for power-law solutions of Eqs. (49)–(52) at small values of p. Given that we have four coupled first-order o.d.e.s, we expect to find four independent power-law solutions. The first solution is such that

$$\bar{Y}(p) = \mathrm{i}\,(Q_E+Q_e)\,a_{-1}\,p^{-1} - \left[\frac{\mathrm{i}}{2}\,Q_E\,(Q_E+Q_e)\,(Q_E+Q_i)+1\right]a_{-1}\,p + \mathcal{O}(p^3), \tag{53}$$

$$\bar{N}(p) = -\mathrm{i}\,Q_e\,a_{-1}\,p^{-1} + \frac{\mathrm{i}}{2}\,Q_E\,Q_e\,(Q_E+Q_i)\,a_{-1}\,p + \mathcal{O}(p^3), \tag{54}$$

$$\bar{J}(p) = -a_{-1} - \frac{1}{2}\,Q_E\,(Q_E+Q_i)\,a_{-1}\,p^2 + \mathcal{O}(p^4), \tag{55}$$

$$\bar{V}(p) = -\frac{[\,\mathrm{i}\,Q_e\,(1+P_E) + Q_E\,(Q_E+Q_i)\,D^2]}{2\,c_\beta^2}\,a_{-1}\,p^2 + \mathcal{O}(p^4), \tag{56}$$

where a_{-1} is an arbitrary constant. The second solution is such that

$$\bar{Y}(p) = \mathrm{i}\,(Q_E+Q_e)\,a_0 - \frac{\mathrm{i}}{6}\,Q_E\,(Q_E+Q_e)\,(Q_E+Q_i)\,a_0\,p^2 + \mathcal{O}(p^4), \tag{57}$$

$$\bar{N}(p) = -\mathrm{i}\,Q_e\,a_0 + \frac{\mathrm{i}}{6}\,Q_E\,Q_e\,(Q_E+Q_i)\,a_0\,p^2 + \mathcal{O}(p^4), \tag{58}$$

$$\bar{J}(p) = -\frac{1}{3}\,Q_E\,(Q_E+Q_i)\,a_0\,p^3 + \mathcal{O}(p^5), \tag{59}$$

$$\bar{V}(p) = -\frac{1}{3}\,\frac{[\,\mathrm{i}\,Q_e\,P_E + Q_E\,(Q_E+Q_i)\,D^2]}{c_\beta^2}\,a_0\,p^3 + \mathcal{O}(p^5), \tag{60}$$

where a_0 is an arbitrary constant. The third solution is such that

$$\bar{Y}(p) = -\frac{1}{6}\,(Q_E+Q_e)\,(Q_E+Q_i)\,a_2\,p^2 + \mathcal{O}(p^4), \tag{61}$$

$$\bar{N}(p) = a_2 + \frac{\mathrm{i}}{2}\,(Q_E+Q_i)\left(-\frac{\mathrm{i}}{3}\,Q_e + \frac{g}{c_\beta^2}\right)a_2\,p^2 + \mathcal{O}(p^4), \tag{62}$$

$$\bar{J}(p) = \frac{\mathrm{i}}{3}\,(Q_E+Q_i)\,a_2\,p^3 + \mathcal{O}(p^5), \tag{63}$$

$$\bar{V}(p) = \mathrm{i}\,\frac{(Q_E+Q_e)}{c_\beta^2}\,a_2\,p + \mathcal{O}(p^3), \tag{64}$$

where a_2 is an arbitrary constant. The final solution is such that

$$\bar{Y}(p) = -\frac{\mathrm{i}}{12}\, Q_E\,(Q_E+Q_e)\,(Q_E+Q_i)\, a_3\, p^3 + \mathcal{O}(p^5), \tag{65}$$

$$\bar{N}(p) = -\mathrm{i}\, Q_E\, a_3\, p + \mathcal{O}(p^3), \tag{66}$$

$$\bar{J}(p) = -\frac{1}{4}\, Q_E\,(Q_E+Q_i)\, a_3\, p^4 + \mathcal{O}(p^6), \tag{67}$$

$$\bar{V}(p) = -\frac{Q_E\,(Q_E+Q_e)}{2\,c_\beta^2}\, a_3\, p^2 + \mathcal{O}(p^4), \tag{68}$$

where a_3 is an arbitrary constant. Note, however, that the third solution is not consistent with Eqs. (37)–(40), which mandate that $\bar{N}(p) \rightarrow -[Q_e/(Q_E+Q_e)]\,\bar{Y}(p) + \mathcal{O}(p)$ and $\bar{V}(p) \rightarrow \mathcal{O}(p^2)$ as $p \rightarrow 0$. Hence, we deduce that $a_2 = 0$.

We conclude that, at small values of p, the most general solution for $\bar{Y}(p)$ and $\bar{N}(p)$ takes the form

$$\bar{Y}(p) = \mathrm{i}\,(Q_E+Q_e)\,(a_{-1}\, p^{-1} + a_0) + \mathcal{O}(p), \tag{69}$$

$$\bar{N}(p) = -\mathrm{i}\, Q_e\,(a_{-1}\, p^{-1} + a_0) + \mathcal{O}(p), \tag{70}$$

which is consistent with Eqs. (37)–(40).

A.9 Ricatti matrix differential equation

Let

$$\underline{u} = \begin{pmatrix} \bar{Y} \\ \bar{N} \end{pmatrix}, \tag{71}$$

$$\underline{v} = \begin{pmatrix} \bar{J} \\ c_\beta^2\, \bar{V} \end{pmatrix}. \tag{72}$$

Equations (49)–(52) can be written in the form

$$\frac{d\underline{u}}{dp} = \underline{\underline{A}}\,\underline{v}, \tag{73}$$

$$\frac{d\underline{v}}{dp} = \underline{\underline{B}}\,\underline{u}, \tag{74}$$

where

$$A_{11} = \frac{\mathrm{i}\,(Q_E+Q_e)+p^2}{p^2}, \tag{75}$$

$$A_{12} = 0, \tag{76}$$

$$A_{21} = -\frac{\mathrm{i}\, Q_e}{p^2}, \tag{77}$$

$$A_{22} = \frac{\mathrm{i}\, Q_E + P_\varphi\, p^2}{c_\beta^2}, \tag{78}$$

$$B_{11} = \mathrm{i}\,(Q_E+Q_i)\, p^2 + P_\varphi\, p^4, \tag{79}$$

$$B_{12} = \mathrm{i}\,(Q_E+Q_i)\, p^2 + \iota_e^{-1}\, P_\varphi\, p^4, \tag{80}$$

$$B_{21} = \mathrm{i}\, Q_e + \mathrm{i}\,(Q_E+Q_i)\, D^2\, p^2 + D^2\, P_\varphi\, p^4, \tag{81}$$

$$B_{22} = \mathrm{i}\,(Q_E+Q_e) + [P_E + \mathrm{i}\,(Q_E+Q_i)\, D^2]\, p^2 + \iota_e^{-1}\, D^2\, P_\varphi\, p^4. \tag{82}$$

Thus, we obtain the following matrix differential equation:

$$\frac{d}{dp}\left(\underline{\underline{A}}^{-1}\,\frac{d\underline{u}}{dp}\right) = \underline{\underline{B}}\,\underline{u}. \tag{83}$$

Let

$$p\,\frac{d\underline{u}}{dp} = \underline{\underline{W}}\,\underline{u}. \tag{84}$$

The previous two equations can be combined to give

$$\left(p\,\frac{d\underline{\underline{W}}}{dp} - \underline{\underline{W}} + \underline{\underline{W}}\,\underline{\underline{W}} + \underline{\underline{A}}\,p\,\frac{d\underline{\underline{A}}^{-1}}{dp}\,\underline{\underline{W}} - p^2\,\underline{\underline{A}}\,\underline{\underline{B}}\right)\underline{u} = \underline{0}, \tag{85}$$

which yields the Riccati matrix differential equation,

$$p\,\frac{d\underline{\underline{W}}}{dp} = \underline{\underline{W}} - \underline{\underline{W}}\,\underline{\underline{W}} - \underline{\underline{E}}\,\underline{\underline{W}} + \underline{\underline{F}}, \tag{86}$$

where

$$\underline{\underline{E}}(p) = \underline{\underline{A}}\,p\,\frac{d\underline{\underline{A}}^{-1}}{dp}, \tag{87}$$

$$\underline{\underline{F}}(p) = p^2\,\underline{\underline{A}}\,\underline{\underline{B}}. \tag{88}$$

In fact, it is easily demonstrated that

$$E_{11} = \frac{2\,\mathrm{i}\,(Q_E + Q_e)}{\mathrm{i}\,(Q_E + Q_e) + p^2}, \tag{89}$$

$$E_{12} = 0, \tag{90}$$

$$E_{21} = -\frac{2\,\mathrm{i}\,Q_e\,(\mathrm{i}\,Q_E + 2\,P_\varphi\,p^2)}{[\mathrm{i}\,(Q_E + Q_e) + p^2]\,(\mathrm{i}\,Q_E + P_\varphi\,p^2)}, \tag{91}$$

$$E_{22} = -\frac{2\,P_\varphi\,p^2}{\mathrm{i}\,Q_E + P_\varphi\,p^2}, \tag{92}$$

and

$$F_{11} = p^2\,[\mathrm{i}\,(Q_E + Q_e) + p^2]\,[\mathrm{i}\,(Q_E + Q_i) + P_\varphi\,p^2], \tag{93}$$

$$F_{12} = p^2\,[\mathrm{i}\,(Q_E + Q_e) + p^2]\,[\mathrm{i}\,(Q_E + Q_i) + \iota_e^{-1}\,P_\varphi\,p^2], \tag{94}$$

$$\begin{aligned} F_{21} = {} & -\mathrm{i}\,Q_e\,p^2\,[\mathrm{i}\,(Q_E + Q_i) + P_\varphi\,p^2] \\ & + c_\beta^{-2}\,p^2\,(\mathrm{i}\,Q_E + P_\varphi\,p^2)\,[\mathrm{i}\,Q_e + \mathrm{i}\,(Q_E + Q_i)\,D^2\,p^2 + D^2\,P_\varphi\,p^4], \end{aligned} \tag{95}$$

$$\begin{aligned} F_{22} = {} & -\mathrm{i}\,Q_e\,p^2\,[\mathrm{i}\,(Q_E + Q_i) + \iota_e^{-1}\,P_\varphi\,p^2] \\ & + c_\beta^{-2}\,p^2\,(\mathrm{i}\,Q_E + P_\varphi\,p^2)\,\{\mathrm{i}\,(Q_E + Q_e) + [P_E + \mathrm{i}\,(Q_E + Q_i)\,D^2]\,p^2 + \iota_e^{-1}\,D^2\,P_\varphi\,p^4\}. \end{aligned} \tag{96}$$

Finally, if

$$\underline{\underline{W}}(p) = \begin{pmatrix} W_{11}, & W_{12} \\ W_{21}, & W_{22} \end{pmatrix} \tag{97}$$

then Eq. (86) yields

$$p\,\frac{dW_{11}}{dp} = W_{11} - W_{11}\,W_{11} - W_{12}\,W_{21} - E_{11}\,W_{11} + F_{11}, \tag{98}$$

$$p\,\frac{dW_{12}}{dp} = W_{12} - W_{11}\,W_{12} - W_{12}\,W_{22} - E_{11}\,W_{12} + F_{12}, \tag{99}$$

$$p\,\frac{dW_{21}}{dp} = W_{21} - W_{21}\,W_{11} - W_{22}\,W_{21} - E_{21}\,W_{11} - E_{22}\,W_{21} + F_{21}, \tag{100}$$

$$p\,\frac{dW_{22}}{dp} = W_{22} - W_{21}\,W_{12} - W_{22}\,W_{22} - E_{21}\,W_{12} - E_{22}\,W_{22} + F_{22}. \tag{101}$$

Thus, our final system of equations consists of a set of four coupled nonlinear differential equations.

A.10 Small-argument behavior of Riccati matrix differential equation

It follows from Eqs. (89)–(92) that $\underline{\underline{E}}(p) = \underline{\underline{E}}^{\,(0)} + \mathcal{O}(p^2)$ at small values of p, where

$$E_{11}^{(0)} = 2, \tag{102}$$

$$E_{12}^{(0)} = 0, \tag{103}$$

$$E_{21}^{(0)} = -\frac{2\,Q_e}{Q_E + Q_e}, \tag{104}$$

$$E_{22}^{(0)} = 0. \tag{105}$$

Likewise, Eqs. (93)–(96) imply that $\underline{\underline{F}}(p) = \mathcal{O}(p^2)$.

Suppose that $\underline{\underline{W}}(p) = \underline{\underline{W}}^{\,(0)} + \underline{\underline{W}}^{\,(1)}\,p$ at small values of p, where the elements of $\underline{\underline{W}}^{\,(0)}$ and $\underline{\underline{W}}^{\,(1)}$ are independent of p. Equation (86) gives

$$\underline{\underline{0}} = \underline{\underline{W}}^{\,(0)} - \underline{\underline{W}}^{\,(0)}\,\underline{\underline{W}}^{\,(0)} - \underline{\underline{E}}^{\,(0)}\,\underline{\underline{W}}^{\,(0)}, \tag{106}$$

$$\underline{\underline{0}} = -\underline{\underline{W}}^{\,(1)}\,\underline{\underline{W}}^{\,(0)} - \underline{\underline{W}}^{\,(0)}\,\underline{\underline{W}}^{\,(1)} - \underline{\underline{E}}^{\,(0)}\,\underline{\underline{W}}^{\,(1)}. \tag{107}$$

Suitable solutions are

$$\underline{\underline{W}}^{\,(0)} = \begin{pmatrix} -1, & 0 \\ -E_{21}^{(0)}/2, & 0 \end{pmatrix}, \tag{108}$$

$$W_{12}^{(1)} = 0, \tag{109}$$

$$W_{21}^{(1)} = \frac{E_{21}^{(0)}}{2}\left[W_{11}^{(1)} - W_{22}^{(1)}\right]. \tag{110}$$

At small values of p, let

$$\underline{u}(p) = \underline{u}_{-1}\,p^{-1} + \underline{u}_0, \tag{111}$$

where the elements of $\underline{u}_{-1}$ (which are y_{-1} and n_{-1}, respectively) and the elements of $\underline{u}_0$ (which are y_0 and n_0, respectively) are all constants. Equation (84) gives

$$\underline{\underline{W}}^{\,(0)}\,\underline{u}_{-1} = -\underline{u}_{-1}, \tag{112}$$

$$\underline{\underline{W}}^{\,(0)}\,\underline{u}_0 + \underline{\underline{W}}^{\,(1)}\,\underline{u}_{-1} = \underline{0}. \tag{113}$$

Thus, making use of Eq. (108), we get

$$\begin{pmatrix} -1, & 0 \\ -E_{21}^{(0)}/2, & 0 \end{pmatrix} \begin{pmatrix} y_{-1} \\ n_{-1} \end{pmatrix} = - \begin{pmatrix} y_{-1} \\ n_{-1} \end{pmatrix}, \tag{114}$$

which implies that

$$\frac{E_{21}^{(0)}}{2}\, y_{-1} = -\frac{Q_e}{Q_E + Q_e}\, y_{-1} = n_{-1}, \tag{115}$$

in accordance with Eqs. (69) and (70), where use has been made of Eq. (104). Equations (108)–(110) and (113) yield

$$\frac{y_0}{y_{-1}} = W_{11}^{(1)}, \tag{116}$$

with n_0 undetermined. It follows from Equation (47) that

$$\frac{\pi}{\hat{\Delta}} \equiv \frac{y_0}{y_{-1}} = W_{11}^{(1)} = \frac{dW_{11}(0)}{dp}. \tag{117}$$

Note, incidentally, that the result $\pi/\hat{\Delta} = y_0/y_{-1}$ follows directly from Eq. (33), and would hold even if a_2 were non-zero.

A.11 Large-argument behavior of Riccati matrix differential equation

At large values of p, it is clear from Eqs. (93)–(96) that $\underline{\underline{F}}(p) = \underline{\underline{F}}^{(6)}\, p^6 + \underline{\underline{F}}^{(8)}\, p^8$, where the elements of $\underline{\underline{F}}^{(6)}$ and $\underline{\underline{F}}^{(8)}$ are independent ot p. On the other hand, Eqs. (89)–(92) imply that $\underline{\underline{E}}(p) = \underline{\underline{E}}^{(0)}$, where the elements of $\underline{\underline{E}}^{(0)}$ are independent of p. Thus, if we write $\underline{\underline{W}}(p) = \underline{\underline{W}}^{(2)}\, p^2 + \underline{\underline{W}}^{(4)}\, p^4$, where the elements of $\underline{\underline{W}}^{(2)}$ and $\underline{\underline{W}}^{(4)}$ are independent of p, then Eq. (86) gives

$$\underline{\underline{W}}^{(4)}\, \underline{\underline{W}}^{(4)} = \underline{\underline{F}}^{(8)}, \tag{118}$$

$$\underline{\underline{W}}^{(2)}\, \underline{\underline{W}}^{(4)} + \underline{\underline{W}}^{(4)}\, \underline{\underline{W}}^{(2)} = \underline{\underline{F}}^{(6)}. \tag{119}$$

Now, according to Eqs. (93)–(96),

$$F_{11}^{(8)} = 0, \tag{120}$$

$$F_{12}^{(8)} = 0, \tag{121}$$

$$F_{21}^{(8)} = c_\beta^{-2}\, D^2\, P_\varphi^2, \tag{122}$$

$$F_{22}^{(8)} = c_\beta^{-2}\, \iota_e^{-1}\, D^2\, P_\varphi^2, \tag{123}$$

so Eq. (118) yields

$$W_{11}^{(4)} = 0, \tag{124}$$

$$W_{12}^{(4)} = 0, \tag{125}$$

$$W_{21}^{(4)} = -c_\beta^{-1}\, \iota_e^{1/2}\, D\, P_\varphi, \tag{126}$$

$$W_{22}^{(4)} = -c_\beta^{-1}\, \iota_e^{-1/2}\, D\, P_\varphi, \tag{127}$$

where we have chosen the sign of the square root that is associated with well-behaved solutions at large values of p. Here, we are assuming that $\iota_e > 0$. Equations (93)–(96) also give

$$F_{11}^{(6)} = P_\varphi, \tag{128}$$

$$F_{12}^{(6)} = \iota_e^{-1}\, P_\varphi, \tag{129}$$

$$F_{21}^{(6)} = \mathrm{i}\, c_\beta^{-2}\, Q_E\, D^2\, P_\varphi + \mathrm{i}\, c_\beta^{-2}\, (Q_E + Q_i)\, D^2\, P_\varphi, \tag{130}$$

$$F_{22}^{(6)} = \mathrm{i}\, c_\beta^{-2}\, \iota_e^{-1}\, Q_E\, D^2\, P_\varphi + c_\beta^{-2}\, [P_E + \mathrm{i}\, (Q_E + Q_i)\, D^2]\, P_\varphi. \tag{131}$$

Thus, Eq. (119) yields

$$W_{12}^{(2)}\, W_{21}^{(4)} = F_{11}^{(6)}, \tag{132}$$

$$W_{12}^{(2)}\, W_{22}^{(4)} = F_{12}^{(6)}, \tag{133}$$

which gives

$$W_{12}^{(2)} = -c_\beta\, \iota_e^{-1/2}\, D^{-1}. \tag{134}$$

Now, if

$$\underline{\underline{W}}\, \underline{u} = \lambda(p)\, \underline{u} \tag{135}$$

then Eq. (84) yields

$$p\, \frac{d\underline{u}}{dp} = \lambda\, \underline{u}, \tag{136}$$

which implies that

$$\underline{u}(p) = \underline{u}(p_0)\, \exp\left[\int_{p_0}^{p} \frac{\lambda_r(p')}{p'}\, dp'\right] \exp\left[\mathrm{i} \int_{p_0}^{p} \frac{\lambda_i(p')}{p'}\, dp'\right], \tag{137}$$

where λ_r and λ_i are the real and imaginary parts of λ, respectively. Of course, a solution that is well behaved at large values of p is such that λ_r is negative. As we have seen, the large-p limit of Eq. (86) is

$$\underline{\underline{W}}\, \underline{\underline{W}} = \underline{\underline{F}}. \tag{138}$$

Hence, if

$$\underline{\underline{F}}\, \underline{u} = \Lambda\, \underline{u} \tag{139}$$

then Eqs. (135) and (139) imply that

$$\lambda^2 = \Lambda. \tag{140}$$

The eigenvalue problem for the F-matrix reduces to

$$\Lambda^2 - (F_{11} + F_{22})\, \Lambda + F_{11}\, F_{22} - F_{12}\, F_{21} = 0. \tag{141}$$

Now,

$$F_{11} + F_{22} \simeq F_{22}^{(8)}\, p^8 = c_\beta^{-2}\, \iota_e^{-1}\, D^2\, P_\varphi^2\, p^8, \tag{142}$$

$$\begin{aligned} F_{11}\, F_{22} - F_{12}\, F_{21} &\simeq \left[F_{11}^{(6)}\, F_{22}^{(8)} - F_{12}^{(6)}\, F_{21}^{(8)}\right] p^{14} \\ &\quad + \left[F_{11}^{(6)}\, F_{22}^{(6)} - F_{12}^{(6)}\, F_{21}^{(6)}\right] p^{12} = c_\beta^{-2}\, R\, P_\varphi^2\, p^{12}, \end{aligned} \tag{143}$$

where

$$R = P_E + \mathrm{i}\, (1 - \iota_e^{-1})\, (Q_E + Q_i)\, D^2, \tag{144}$$

Hence, the two eigenvalues of the F-matrix are

$$\Lambda_1 \simeq F_{22}^{(8)}\, p^8 = c_\beta^{-2}\, \iota_e^{-1}\, D^2\, P_\varphi^2\, p^8, \tag{145}$$

$$\Lambda_2 \simeq \frac{[F_{11}^{(6)}\, F_{22}^{(6)} - F_{12}^{(6)}\, F_{21}^{(6)}]}{F_{22}^{(8)}}\, p^4 = \iota_e\, D^{-2}\, R\, p^4. \tag{146}$$

Thus, we deduce that the two eigenvalues of the W-matrix are

$$\lambda_1 = -\Lambda_1^{1/2} = -c_\beta^{-1}\, \iota_e^{-1/2}\, D\, P_\varphi\, p^4, \tag{147}$$

$$\lambda_2 = -\Lambda_2^{1/2} = -\iota_e^{1/2}\, D^{-1}\, R^{1/2}\, p^2, \tag{148}$$

Here, the square root of R is taken such that the real part of λ_2 is negative. Now, the eigenvalue problem for the W-matrix reduces to

$$\lambda^2 - W_{22}^{(4)}\, p^4\, \lambda + \left[W_{11}^{(2)}\, W_{22}^{(4)} - W_{12}^{(2)}\, W_{21}^{(4)}\right] p^6 = 0. \tag{149}$$

which yields

$$\lambda_1 \simeq W_{22}^{(4)}\, p^4, \tag{150}$$

which is in agreement with Eq. (147), and

$$\lambda_2 \simeq \left[W_{11}^{(2)} - \frac{W_{12}^{(2)}\, W_{21}^{(4)}}{W_{22}^{(4)}}\right] p^2, \tag{151}$$

which implies that

$$W_{11}^{(2)} = -\iota_e^{1/2}\, D^{-1}\, R^{1/2} - c_\beta\, \iota_e^{1/2}\, D^{-1}. \tag{152}$$

Hence, the large-p boundary condition for the W-matrix is

$$\underline{\underline{W}}(p) = \begin{pmatrix} -\iota_e^{1/2}\, D^{-1}\, R^{1/2}\, p^2 - c_\beta\, \iota_e^{1/2}\, D^{-1}\, p^2, & -c_\beta\, \iota_e^{-1/2}\, D^{-1}\, p^2 \\ -c_\beta^{-1}\, \iota_e^{1/2}\, D\, P_\varphi\, p^4, & -c_\beta^{-1}\, \iota_e^{-1/2}\, D\, P_\varphi\, p^4 \end{pmatrix}. \tag{153}$$

A.12 Method of solution

The method of solution is to launch the well-behaved asymptotic solution (153) of Eqs. (98)–(101) from large p, and then integrate the equations backward to small p. The scaled layer response index, $\hat{\Delta}$, is then determined from Eq. (117). Note that, because there are no free parameters in expression (153), the scaled layer response index is uniquely determined by this procedure. Finally, the true layer response index is given by $\Delta_s = S^{1/3}\, \hat{\Delta}$. [See Eq. (41).]

References

[1] J.T. Scoville, R.J. La Haye, A.G. Kellman, T.H. Osborne, R.D. Stambaugh, E.J. Strait and T.S. Taylor, *Locked modes in DIII-D and a method for prevention of the low density mode*, Nucl. Fusion **31**, 875 (1991).

[2] T.C. Hender, R. Fitzpatrick, A.W. Morris, P.G. Carolan, R.D. Durst, T. Edlington, J. Ferreira, S.J. Fielding, P.S. Haynes, J. Hugill, et al., *Effect of resonant magnetic perturbations on COMPASS-C tokamak discharges*, Nucl. Fusion **32**, 2091 (1992).

[3] G.M. Fishpool and P.S. Haynes, *Field error instabilities in JET*, Nucl. Fusion **34**, 109 (1994).

[4] R. Fitzpatrick, *Interaction of tearing modes with external structures in cylindrical geometry (plasma)*, Nucl. Fusion **33**, 1049 (1993).

[5] R. Fitzpatrick, *Bifurcated states of a rotating tokamak plasma in the presence of a static error-field*, Phys. Plasmas **5**, 3325 (1998).

[6] M. Pharr, N.C. Logan, C. Paz-Soldan, J.-K. Park and C. Hansen, *Error field predictability and consequences for ITER*, Nucl. Fusion **64**, 126025 (2024).

[7] T.E. Evans, R.A. Moyer, J.G. Watkins, P.R. Thomas, T.H. Osborne, J.A. Boedo, M.E. Fenstermacher, K.H. Finken, R.J. Groebner, M. Groth, et al., *Suppression of large edge-localized modes in high-confinement DIII-D plasmas with a stochastic magnetic boundary*, Phys. Rev. Lett. **92**, 235003 (2004).

[8] A.H. Boozer, *Physics of magnetically confined plasmas*, Rev. Mod. Phys. **76**, 1071 (2004).

[9] Z. Chang and J.D. Callen, *Global energy confinement degradation due to macroscopic phenomena in tokamaks*, Nucl. Fusion **30**, 219 (1990).

[10] H.P. Furth, J. Killeen and M.N. Rosenbluth, *Finite-resistivity instabilities of a sheet pinch*, Phys. Fluids **6**, 459 (1963).

[11] G. Ara, B. Basu, B. Coppi, G. Laval, M.N. Rosenbluth and B.V. Waddell, *Magnetic reconnection and $m = 1$ oscillations in current carrying plasmas*, Ann. Phys. (NY) **112**, 443 (1978).

[12] J.F. Drake and Y.C. Lee, *Kinetic theory of tearing instabilities*, Phys. Fluids **20**, 1341 (1977).

[13] F.L. Waelbroeck, *Shielding of resonant magnetic perturbations in the long mean-free-path regime*, Phys. Plasmas **10**, 4040 (2003).

[14] A. Cole and R. Fitzpatrick, *Drift-magnetohydrodynamical model of error-field penetration in tokamak plasmas*, Phys. Plasmas **13**, 032503 (2006).

[15] R. Fitzpatrick and F.L. Waelbroeck, *Two-fluid magnetic island dynamics in slab geometry. I. Isolated islands*, Phys. Plasmas **12**, 022307 (2005).

[16] R.D. Hazeltine, M. Kotschenreuther and P.G. Morrison, *A four-field model for tokamak plasma dynamics*, Phys. Fluids **28**, 2466 (1985).

[17] R. Fitzpatrick, *Influence of anomalous perpendicular transport on linear tearing mode dynamics in tokamak plasmas*, Phys. Plasmas **29**, 032507 (2022).

[18] Y. Lee, J.-K. Park and Y.-S. Na, *Effect of parallel flow on resonant layer responses in high beta plasmas*, Nucl. Fusion **64**, 106058 (2024).

[19] D.P. Brennan, A.J. Cole, C. Akcay and J.M. Finn, *Two fluid stability of rotating tokamak plasmas using machine learning*, Bul. Am. Phys. Soc. **64**, 249 (2019).

[20] J.-K. Park, *Parametric dependencies of resonant layer responses across linear, two-fluid, drift-MHD regimes*, Phys. Plasmas **29**, 072506 (2022).

[21] R. Fitzpatrick, *Tearing mode dynamics in tokamak plasmas*, (IOP Publishing, Bristol UK, 2023).

[22] C. Paz-Soldan, R. Nazikian, L. Cui, B.C. Lyons, D.M. Orlov, A. Kirk, N.C. Logan, T.H. Osborne, W. Suttrop and D.B. Weisberg, *The effect of plasma shape and neutral beam mix on the rotation threshold for RMP-ELM suppression*, Nucl. Fusion **59**, 056012 (2019).

[23] R. Fitzpatrick, *Response of a magnetically diverted tokamak plasma to a resonant magnetic perturbation*, arXiv 2511.07666 (2025).

[24] H.P. Furth, P.H. Rutherford and H. Selberg, *Tearing mode in the cylindrical tokamak*, Phys. Fluids **16**, 1054 (1973).

[25] J.A. Wesson, *Hydromagnetic stability of tokamaks*, Nucl. Fusion **18**, 87 (1978).

[26] R. Fitzpatrick, *Calculation of tearing mode stability in an inverse aspect-ratio expanded tokamak plasma equilibrium*, Phys. Plasmas **31**, 102507 (2024).

[27] R. Fitzpatrick, *Investigation of tearing mode stability near ideal stability boundaries via asymptotic matching techniques*, Phys. Plasmas **32**, 062509 (2025).

[28] R.D. Hazeltine and J.D. Meiss, *Plasma confinement*, (Dover, New York NY, 2003).